Coupled-wave formalism for bound states in the continuum in guided-mode resonant gratings

Dmitry A. Bykov,* Evgeni A. Bezus, and Leonid L. Doskolovich
IPSI RAS–Branch of the FSRC "Crystallography and Photonics" RAS, 151 Molodogvardeyskaya Street, Samara 443001, Russia and Samara National Research University, 34 Moskovskoye Shosse, Samara 443086, Russia

(Received 7 March 2019; published 4 June 2019)

We present simple yet extremely accurate coupled-wave models describing the formation of bound states in the continuum (BICs) in one-dimensional periodic guided-mode resonant gratings consisting of a slab waveguide layer with a binary grating attached to one or both of its interfaces. Using these models, we obtain simple closed-form expressions predicting the locations of the BICs and quasi-BICs in the ω-k_x parameter space. We study two mechanisms of the BIC formation: coupling between two counterpropagating guided modes and coupling between a guided mode and a Fabry-Pérot mode. The BIC conditions corresponding to the considered mechanisms are formulated in terms of the scattering coefficients of the binary grating. The predictions of the presented models are in excellent agreement with the results of full-wave simulations obtained using the Fourier modal method.

DOI: 10.1103/PhysRevA.99.063805

I. INTRODUCTION

In recent years, the investigation of bound states in the continuum (BICs) has attracted a great deal of attention. Bound states in the continuum were for the first time theoretically predicted by von Neumann and Wigner for an electronic system with an artificially tailored potential [1]. In the past decade, BICs were discovered and studied in various photonic structures [2]. In contrast to the conventional bound states, BICs are the eigenmodes that, although supported by a structure with open scattering channels, remain perfectly confined, i.e., have an infinite lifetime and an infinite quality factor. There are different mechanisms preventing the leakage of the mode energy to the open channels, including symmetry mismatch [2] and destructive interference of resonances [3].

Photonic BICs were studied in various periodic structures (diffraction gratings, photonic crystal slabs, and infinite arrays of dielectric rods or spheres) [4–19], in defects and interfaces of photonic crystals [20–22], in arrays of optical waveguides [23–25], and in photonic rib waveguides [26,27], among others [2]. Recently, the topological nature of BICs was unveiled [16–18,28], which in particular explained their robustness and led to the discovery of the so-called strong resonances [17–19,28] occurring when two BICs coalesce. The phenomenon of a BIC not only is of great theoretical interest, but has a wide range of practical applications, since a small perturbation in the parameters of the structure or of the incident radiation leads to the collapse of a BIC to a Fano resonance with an extremely high quality factor. The design of high-Q resonators is important, in particular, for the development of lasers [29–31], sensors [32,33], and filters [34].

Periodic optical structures such as diffraction gratings or photonic crystal slabs (PCSs) constitute one of the basic building blocks of photonics. For these structures, advanced theoretical models and efficient numerical methods giving deep insight into their optical properties have been developed. The interest in diffraction gratings and PCSs is due to the fact that they exhibit a wide range of optical phenomena. In particular, most of the known *resonant* effects arising in optics and photonics can be investigated by studying diffraction gratings. It is thus not a surprise that, starting from the pioneering paper [4], the vast majority of the published papers studying photonic BICs focuses on gratings and other periodic structures [4–19]. In Ref. [4], BICs arising due to Fabry-Pérot interference between a pair of resonant gratings were studied theoretically and numerically. Extensive numerical [5–8] and experimental [9] investigations of BICs in structures with one-dimensional (1D) periodicity were carried out. In particular, field enhancement effects near BICs were discussed in Ref. [8]. In Ref. [10], an experimental study of a PCS with 2D periodicity was presented. A recent work [11] demonstrated the existence of quasi-BICs resulting from the coupling of waveguide and plasmonic modes in a metallic grating located on a slab waveguide. Simple approximate models for the BICs based on power series expansion were proposed in Refs. [12–14]. In particular, in Refs. [12,13], the case of symmetry-protected BICs in a PCS with 1D periodicity was considered. In a recent paper, BICs in low-contrast PCSs were theoretically described using Fourier series expansion of the dielectric permittivity [15].

In this paper we investigate BICs and quasi-BICs supported by binary gratings located on the surface of a slab waveguide [Figs. 1(a) and 1(b)]. We will refer to these structures as guided-mode resonant gratings (GMRGs). The eigenmodes of the GMRGs considered in the present work arise due to interference of plane waves inside the waveguide layer. This allows us to formulate simple coupled-wave models describing the optical properties of the GMRGs. The developed models do not utilize series expansion techniques,

*bykovd@gmail.com

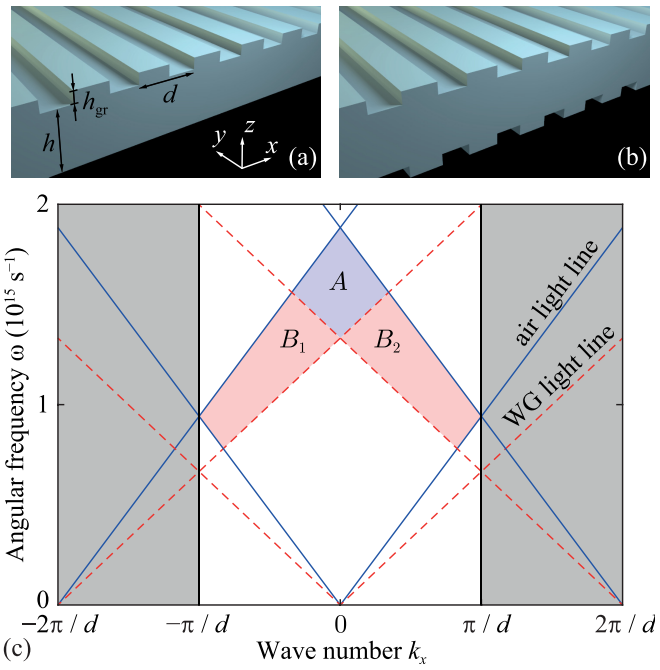

FIG. 1. Guided-mode resonant gratings consisting of a slab waveguide layer with a binary grating attached to (a) one or (b) both of its interfaces. (c) Light lines of ±1st and 0th diffraction orders in the substrate and superstrate (blue solid lines) and in the waveguide layer (red dashed lines).

which makes them extremely accurate. Using these models, we derive simple closed-form expressions predicting the locations of the BICs in the ω-k_x parameter space. We investigate two different mechanisms of BIC formation: coupling of two counterpropagating waveguide modes and coupling of a waveguide mode with a Fabry-Pérot mode.

The paper is organized in five sections. Following the Introduction, Sec. II describes the geometry of the considered structure and revisits some basic aspects of the grating theory. In Sec. III we study BICs and quasi-BICs arising due to coupling of two counterpropagating waveguide modes, which happen near the center of the first Brillouin zone. In Sec. IV we study BICs caused by coupling of a waveguide mode with a Fabry-Pérot mode. Section V summarizes the paper and offers an outlook for future work.

II. THE GMRG GEOMETRY

Let us start with the guided-mode resonant grating shown in Fig. 1(a). The considered GMRG consists of a binary grating with period d placed on top of a slab waveguide with thickness h and refractive index n. The refractive indices of the superstrate and substrate materials are assumed to be unity. The binary grating is assumed to be nonresonant, i.e., all the resonances (and the eigenmodes) of the GMRG arise due to multiple reflections of waves inside the waveguide (WG) layer. The eigenmodes can be excited by an incident plane wave, which is defined by the angular frequency ω and the in-plane wave-vector component $k_x = k_0 \sin\theta$, where θ is the angle of incidence and $k_0 = \omega/c$ is the free-space wave number. Let us note that in the present work we consider only the case of planar diffraction ($k_y = 0$).

We will assume that the grating is subwavelength, i.e., that only the 0th diffraction orders exist in the substrate and superstrate regions. However, inside the WG layer, which has a higher refractive index compared to the substrate (superstrate), several diffraction orders may propagate. For the mth diffraction order inside the WG layer, the x component of the wave vector reads

$$k_{x,m} = k_x + \frac{2\pi}{d} m. \tag{1}$$

The z component of the wave vector has the value

$$k_{z,m} = \sqrt{k_0^2 n^2 - k_{x,m}^2}, \tag{2}$$

which is real for the propagating diffraction orders and imaginary for the evanescent ones.

Figure 1(c) shows the light lines (light cones) of the 0th and ±1st diffraction orders in the substrate (superstrate) and in the WG layer. In the shaded regions marked A and $B_{1,2}$, the substrate and superstrate support only the 0th diffraction order, whereas in the WG layer, also the ±1st diffraction orders propagate. In region A, both −1st and +1st orders exist in the waveguide layer, while in regions $B_{1,2}$ only one of these diffraction orders is present. Regions A and $B_{1,2}$ are the regions where GMRGs exhibit pronounced resonant properties, which allows one to use GMRGs as optical filters known as guided-mode resonant filters.

In Sec. III we consider BICs and quasi-BICs supported by the GMRG operating in region A. In Sec. IV we will focus on regions $B_{1,2}$.

III. BOUND STATES IN THE CONTINUUM AND QUASI-BICS EMERGING FROM COUPLING OF TWO WAVEGUIDE MODES

A. Coupled-wave model

In this section we present a coupled-wave model of the GMRG operating in region A [see Fig. 1(c)]. This model allows us to obtain simple expressions for the transmission and reflection spectra of the GMRG. As we show below, analysis of these expressions enables predicting the positions of the BICs and quasi-BICs in the ω-k_x plane.

To formulate the coupled-wave model, we consider only the propagating diffraction orders (plane waves) in the superstrate, substrate, and WG layer of the GMRG. In doing so, we assume that the WG layer is thick enough so that the near-field interactions between its interfaces caused by the evanescent diffraction orders can be neglected. The considered propagating plane waves are shown with arrows in Fig. 2. The field in the superstrate comprises two plane waves: the incident wave I and the reflected wave R. The field in the WG layer is represented by four plane waves: the ±1st diffraction orders (U_1 and V_1) and the same plane waves after total internal reflection from the lower interface of the WG layer (U_2 and V_2). The two V waves constitute the rightward-propagating mode of the waveguide. Similarly, the two U waves form the waveguide mode propagating to the left. We assume that the 0th transmitted diffraction order of the grating goes through

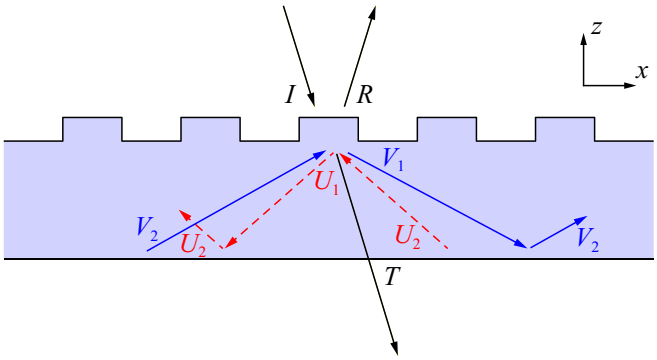

FIG. 2. Propagating plane waves considered in the coupled-wave model.

the lower interface of the WG layer without reflection (Fig. 2), which gives the transmitted wave T. We will discuss the consequences of this assumption later in Sec. III C.

The letters in Fig. 2 denote the complex amplitudes of the considered plane waves. The amplitudes of the incident, reflected, and transmitted plane waves (I, R, and T) are defined at the upper interface of the grating. The amplitudes of the upward-propagating waves inside the waveguide (U_2 and V_2) are defined at the lower interface of the WG layer, whereas the amplitudes of the downward-propagating plane waves (U_1 and V_1) are defined at its upper interface.

The amplitudes of the U waves at the upper and lower interfaces differ by the term $e^{i\phi}$, where the phase is given by $\phi = hk_{z,-1}$. According to Eq. (2), this phase has the form

$$\phi = h\sqrt{k_0^2 n^2 - \left(k_x - \frac{2\pi}{d}\right)^2}. \tag{3}$$

Similarly, the complex amplitudes of the V waves change by $e^{i\psi}$ after propagating between the upper and lower interfaces of the waveguide layer. The phase ψ is given by

$$\psi = h\sqrt{k_0^2 n^2 - \left(k_x + \frac{2\pi}{d}\right)^2}. \tag{4}$$

The plane waves shown in Fig. 2 are coupled by the diffraction grating, which can be described by a 4×4 scattering matrix S,

$$\begin{bmatrix} R \\ T \\ U_1 \\ V_1 \end{bmatrix} = \underbrace{\begin{bmatrix} r & t & d_{ru} & d_{rv} \\ t & \tilde{r} & d_{tu} & d_{tv} \\ d_{ru} & d_{tu} & r_u & c \\ d_{rv} & d_{tv} & c & r_v \end{bmatrix}}_{S} \begin{bmatrix} I \\ 0 \\ U_2 e^{i\phi} \\ V_2 e^{i\psi} \end{bmatrix}, \tag{5}$$

where the zero on the right-hand side means that there is no wave incident from the substrate. The elements of the scattering matrix are the coupling coefficients having the following notation. The letters d, r, and t denote diffraction, reflection, and transmission, respectively. The subscripts in these coefficients denote the scattering channels being coupled. Finally, the coefficient c describes coupling between the U and V waves.

Note that the scattering matrix in Eq. (5) is symmetric due to reciprocity [35]; therefore, it contains only ten unique elements. Let us further note that for a lossless structure, the scattering matrix is unitary [35]. Therefore, the defined coefficients are not arbitrary but are subject to the energy conservation law.

As it is shown in Fig. 2, we assumed that the wave T goes through the lower interface of the waveguide layer without reflection. However, the waves U_1 and V_1 undergo total internal reflection at this interface. By denoting the corresponding reflection coefficients by r'_u and r'_v, we obtain

$$\begin{aligned} U_2 &= r'_u U_1 e^{i\phi}, \\ V_2 &= r'_v V_1 e^{i\psi}. \end{aligned} \tag{6}$$

Let us consider the diffraction of a unity-amplitude incident wave ($I = 1$). In this case, by solving Eqs. (5) and (6) for T, we obtain the following analytical expression for the transmission coefficient of the GMRG:

$$T = t + \frac{d_{rv}d_{tv}(e^{-2i\phi}/r'_u - r_u) + d_{ru}d_{tu}(e^{-2i\psi}/r'_v - r_v) + c(d_{rv}d_{tu} + d_{ru}d_{tv})}{(e^{-2i\phi}/r'_u - r_u)(e^{-2i\psi}/r'_v - r_v) - c^2}. \tag{7}$$

A similar expression can be obtained for the reflection coefficient (complex amplitude of the 0th reflected diffraction order), having the same denominator as in Eq. (7). This denominator describes the eigenmodes of the structure [36]. Although it is not the case considered in the present work, let us note that when the coupling coefficient c vanishes, the denominator turns into the product of two terms corresponding to the *uncoupled* leftward- and rightward-propagating leaky waveguide modes.

B. Bound states in the continuum

In this section, using the approximate Eq. (7), we study the BICs supported by GMRGs operating in region A [see Fig. 1(c)]. However, before discussing the BICs, let us first recall some necessary facts from the theory of resonances.

Usually, resonances in the reflection and transmission spectra are described by a complex frequency ω_p of the corresponding eigenmode of the structure [36]. The complex eigenfrequency can be found as a complex pole of the transmission or reflection coefficients, i.e., by solving the equation $T(\omega_p) = \infty$ or $R(\omega_p) = \infty$ [36]. The real part of ω_p gives the mode excitation frequency. The imaginary part determines the linewidth of the resonance, whereas its inverse, referred to as the lifetime of the resonance, describes the decay rate of the mode.

Bound states in the continuum are the modes with an infinite lifetime and hence with a real frequency. Therefore, the denominator in Eq. (7) must vanish at a real frequency of

the BIC. This seemingly contradicts the energy conservation law: The transmission coefficient (7) would diverge once the denominator vanishes. This contradiction is easily resolved if the BIC conditions result in the vanishing of the numerator as well [14]. In this regard, we will use the following approach to find the BICs: First, we simultaneously equate to zero the numerator and the denominator of the fraction in Eq. (7); then, we check whether the denominator and numerator vanish at a *real* frequency and a *real* wave number k_x.

Let us equate the numerator and the denominator in Eq. (7) to zero. By solving the resulting system with respect to the exponents $e^{i\phi}$ and $e^{i\psi}$, we obtain

$$\begin{aligned} e^{i\phi} &= \pm\frac{1}{\sqrt{r'_u(r_u - cd_{ru}/d_{rv})}}, \\ e^{i\psi} &= \pm\frac{1}{\sqrt{r'_v(r_v - cd_{rv}/d_{ru})}}, \end{aligned} \tag{8}$$

where the plus and minus signs can be chosen independently for $e^{i\phi}$ and $e^{i\psi}$.

If Eqs. (8) describe a BIC, i.e., a real-frequency mode, the phases ϕ and ψ should also be real [see Eqs. (3) and (4)]. Therefore, the left- and hence the right-hand sides of Eqs. (8) should lie on the unit circle in the complex plane. Let us show that this is true in the case of normal incidence of light (at $\theta = 0$).

In the case of normal incidence, the scattering problem is symmetric; hence some of the coupling coefficients coincide, namely, $d_{ru} = d_{rv}$, $d_{tu} = d_{tv}$, $r_u = r_v$, and $r'_u = r'_v$. In addition, the phases ϕ and ψ are equal. In this case, Eqs. (8) take the following form:

$$e^{i\phi} = e^{i\psi} = \pm\frac{1}{\sqrt{r'_u(r_u - c)}}. \tag{9}$$

Let us prove that the fraction on the right-hand side of Eq. (9) lies on the unit circle. The term r'_u is the total-internal-reflection coefficient; hence $|r'_u| = 1$. The second term $r_u - c$ has unit modulus as well, since it is the eigenvalue of the unitary matrix S written for the case of normal incidence. Thus, the exponents $e^{i\phi}$ and $e^{i\psi}$ in Eq. (9) lie on the unit circle and consequently ϕ and ψ, defined by Eqs. (3) and (4), are real. Therefore, we can obtain closed-form expressions for ϕ and ψ by taking the argument of the complex numbers in Eq. (9),

$$\phi = \psi = \pi m - \tfrac{1}{2}\arg\{r'_u(r_u - c)\}, \tag{10}$$

where m is an integer. According to Eq. (3), the phase ϕ is a positive number. Therefore, assuming that the arg value lies within the interval $[0, 2\pi)$, we restrict m to be a positive integer.

Having derived the expressions for ϕ and ψ, we can obtain the values of ω and k_x from Eqs. (3) and (4):

$$\begin{aligned} k_x &= \frac{d}{8\pi h^2}(\phi^2 - \psi^2), \\ \omega &= \frac{c}{n}\sqrt{k_x^2 + \frac{\phi^2 + \psi^2}{2h^2} + \frac{4\pi^2}{d^2}}. \end{aligned} \tag{11}$$

In the case of normal incidence, $\phi = \psi$, $k_x = 0$, and the frequency of the BIC is simply

$$\omega = \frac{c}{n}\sqrt{\frac{\phi^2}{h^2} + \frac{4\pi^2}{d^2}}. \tag{12}$$

C. Discussion of the model

In Sec. III A we made an important assumption when formulating the coupled-wave model: We neglected the reflection of the 0th diffraction order at the lower interface of the WG layer. This makes the obtained Eq. (7) describing the transmission coefficient inaccurate. Surprisingly, the model describing the BICs presented in Sec. III B turns out to be exact. Indeed, since the BICs are nonleaky modes, they have zero-amplitude transmitted field in the 0th diffraction order of the GMRG. Therefore, the amplitude of the 0th diffraction order, which is incident at the lower interface of the waveguide (from inside the WG layer), is zero and hence no reflection of the 0th diffraction order occurs at the WG lower interface. This makes Eqs. (10) and (12) accurate when calculating the BICs.

In the preceding section we obtained the BIC condition in the case of normal incidence of light on a structure having a vertical symmetry plane. Therefore, Eq. (10) describes the well-known case of symmetry-protected BICs [2,13]. In the case of oblique incidence, however, the right-hand sides of Eqs. (8) no longer lie on the unit circle. As a consequence, the BIC condition is violated in the case of oblique incidence and instead of infinite-Q BICs we obtain high-Q resonances: quasi-BICs. As we demonstrate in the next section, the (ω, k_x) positions of these quasi-BICs can still be calculated using Eqs. (11) with the phases ϕ and ψ obtained by taking the argument of Eqs. (8).

Let us note that in order to calculate the BIC positions using Eq. (11) or (12), one needs to find the phases ϕ and ψ, which are defined by Eq. (8) or (9). These phases depend on the elements $d_{ru,rv}$, $r_{u,v}$, and c of the scattering matrix S as well as on the total-internal-reflection coefficients $r'_{u,v}$. These seven coupling coefficients are the parameters of the proposed coupled-wave model. If we are working in a narrow ω-k_x range, the coupling coefficients can be assumed to be constants, which can be estimated by fitting the model spectrum [Eq. (7)] to the numerically calculated transmission spectrum. If the ω-k_x dependence of these coefficients cannot be neglected (as in the example considered below), Eqs. (8) and (11) and Eqs. (9) and (12) become *nonlinear* equations with respect to ω and k_x. Fortunately, these equations can be easily solved using the simple iteration method. We start with some arbitrary values of ω and k_x, e.g., $k_x = 0$ and some ω lying in the frequency range of interest. Then we compute the elements of the scattering matrix S by solving the diffraction problem for the grating lying on the substrate having the refractive index equal to that of the WG layer. Then we calculate the phases ϕ and ψ and refine the values of ω and k_x using Eqs. (11) or Eq. (12). Then we start the next iteration with calculating S and so forth. This iterative process shows good convergence and is stopped when the BIC position changes less than the required tolerance.

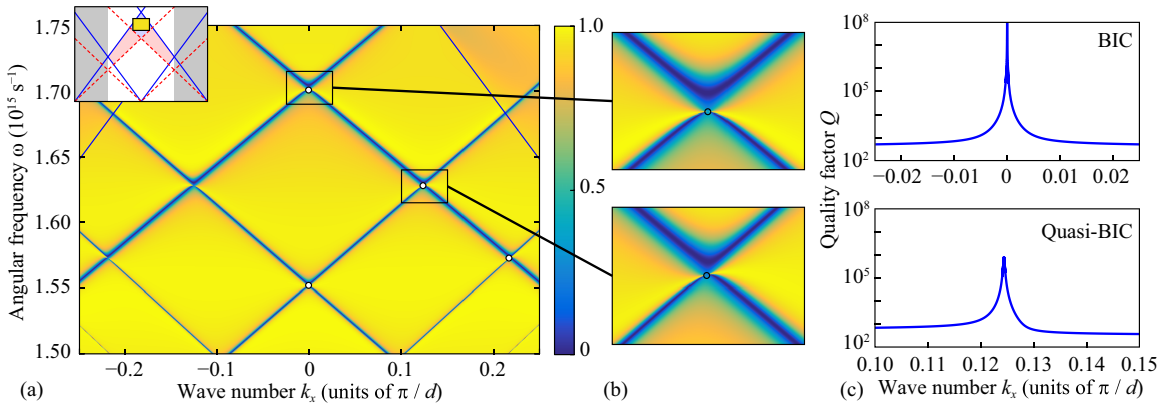

FIG. 3. (a) Rigorously calculated transmission spectrum of the considered GMRG and (b) two magnified fragments demonstrating the formation of a BIC (top panel) and of a quasi-BIC (bottom panel). (c) Quality factors of the modes corresponding to the magnified fragments.

D. Numerical simulations

To confirm the validity of the derived model, we performed full-wave numerical simulations using the Fourier modal method (FMM), which is also known as rigorous coupled-wave analysis [37,38]. The FMM is an established numerical technique for solving Maxwell's equations and is widely used for modeling the diffraction of light by multilayer periodic optical structures. Within this method, the solution of the diffraction problem is reduced to solving an eigenvalue problem in each layer of the structure, followed by solving a system of linear equations describing the boundary conditions at the layer interfaces [37].

Figure 3(a) shows the calculated ω-k_x transmission spectrum of the GMRG with the following parameters: refractive index $n = 1.41$, grating period $d = 1000$ nm, grating height $h_{\mathrm{gr}} = 200$ nm, grating fill factor 50%, and WG layer thickness $h = 2000$ nm. No optimization was performed regarding these parameters. The presented spectrum is calculated in region A as it is shown in the inset of Fig. 3(a).

Figure 3(b) shows two magnified fragments of the spectrum. The top panel shows the BIC region: The resonant line narrows to zero exactly at $k_x = \theta = 0$. The bottom panel corresponds to the case of oblique incidence: A quasi-BIC is expected according to the model.

In order to distinguish BICs from quasi-BICs, we numerically investigated the quality factor of the resonances $Q = \mathrm{Re}\,\omega_{\mathrm{p}}/(-2\,\mathrm{Im}\,\omega_{\mathrm{p}})$ by calculating the complex pole of the scattering matrix of the GMRG obtained using the FMM [36]. Figure 3(c) shows the quality factor calculated along the dispersion curves of the resonances shown in Fig. 3(b). It is evident from Fig. 3(c) that in the case of normal incidence, a BIC is present, whereas in the oblique incidence case, the quality factor of the resonance is finite, which is the evidence of a quasi-BIC.

To verify the presented coupled-wave model, we calculated the predicted positions of the BICs and quasi-BICs. The BIC positions were calculated using Eqs. (10) and (12), whereas the quasi-BIC positions were calculated using Eqs. (8) and (11). The predicted positions of the BICs and quasi-BICs are shown with black circles in Figs. 3(a) and 3(b). For illustrative purposes, we show only the positions of the BICs and quasi-BICs having non-negative wave numbers k_x. Excellent agreement between the predicted (quasi-)BIC positions and the corresponding features in the rigorously calculated spectrum confirms the accuracy of the developed coupled-wave model.

IV. BOUND STATES IN THE CONTINUUM EMERGING FROM COUPLING OF A WAVEGUIDE MODE WITH A FABRY-PÉROT MODE

In the preceding section we considered the coupling of two counterpropagating waveguide modes excited by $\pm$1st diffraction orders, neglecting the reflection of the 0th diffracted order at the lower interface of the WG layer. However, multiple reflections of the 0th order may by themselves result in a resonance, namely, the Fabry-Pérot resonance. In this section we address the question whether the coupling of this Fabry-Pérot mode with a waveguide mode can result in a BIC. We will carry out our analysis for region B_2 [see Fig. 1(c)] (a similar analysis can be performed for region B_1). In region B_2, the waveguide layer supports only two propagating diffraction orders, the 0th and the -1st, whereas the $+1$st diffraction order is evanescent in the WG layer. Similarly to the preceding section, only the 0th diffraction orders propagate in the substrate and superstrate.

The grating of Fig. 1(a) does not support BICs in regions $B_{1,2}$ because the Fabry-Pérot mode leaks out to the substrate via the 0th diffraction order, as we discussed in Sec. III C. In order to obtain BICs, we have to change the scattering behavior of the 0th diffraction order at the lower interface of the structure. We do this by adding the second diffraction grating (having the same geometry) at the lower interface of the waveguide as shown in Fig. 1(b). An alternative approach, not considered in this paper, is to increase the refractive index of the superstrate so that the 0th diffraction channel in the substrate closes before the one in the superstrate does.

A. Coupled-wave model

Let us formulate the coupled-wave model for the structure of Fig. 1(b) by adopting the formalism proposed in Sec. III A. To do this, we define the amplitudes of the plane waves as shown in Fig. 4. Each arrow in Fig. 4 denotes a plane wave.

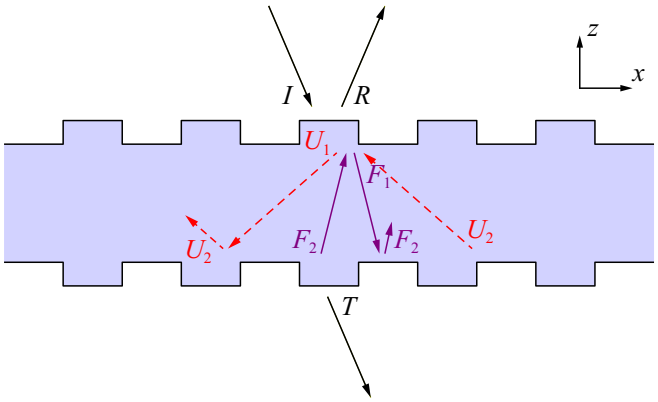

FIG. 4. Propagating plane waves considered in the coupled-wave model of a GMRG with a horizontal symmetry plane.

As before, the letters denote the complex amplitudes of the plane waves. The amplitudes of the incident and reflected plane waves (I and R) are defined at the upper interface of the structure, whereas the amplitude of the transmitted wave T is defined at the lower interface. Inside the waveguide, the amplitudes of the upward-propagating plane waves (U_2 and F_2) are defined at the lower interface of the WG layer, while the amplitudes of the downward-propagating plane waves (U_1 and F_1) are defined at the upper interface. The F waves form the Fabry-Pérot resonance inside the WG layer.

The amplitudes of the U waves at the upper and lower interfaces differ by $e^{i\phi}$, where the phase ϕ is defined by Eq. (3). Similarly, the complex amplitudes of the F waves change by $e^{i\xi}$ when propagating between the upper and lower interfaces of the WG layer. The phase ξ equals $hk_{z,0}$ and, according to Eq. (2), reads

$$\xi = h\sqrt{k_0^2 n^2 - k_x^2}. \tag{13}$$

In the structure of Fig. 4, the plane waves are coupled by both the upper and lower gratings. The upper grating can be described by a unitary 3×3 scattering matrix S:

$$\begin{bmatrix} R \\ F_1 \\ U_1 \end{bmatrix} = \underbrace{\begin{bmatrix} r & t & d_{ru} \\ t & \tilde{r} & d_{tu} \\ d_{ru} & d_{tu} & r_u \end{bmatrix}}_{S} \begin{bmatrix} I \\ F_2 e^{i\xi} \\ U_2 e^{i\phi} \end{bmatrix}. \tag{14}$$

Here the coefficients have the same meaning as in Eq. (5).

Due to the existence of a horizontal symmetry plane, the coupling of plane waves by the lower diffraction grating is described by the very same 3×3 scattering matrix S of Eq. (14):

$$\begin{bmatrix} T \\ F_2 \\ U_2 \end{bmatrix} = S \begin{bmatrix} 0 \\ F_1 e^{i\xi} \\ U_1 e^{i\phi} \end{bmatrix}. \tag{15}$$

Here zero means that there is no wave incident from the substrate region.

Equations (14) and (15) constitute the coupled-wave model of the considered structure. This model takes into account the coupling between the waveguide mode and the Fabry-Pérot mode, i.e., between the 0th and -1st diffraction orders, which is described by the coefficient d_{tu}. By solving the obtained coupled-wave equations with respect to T at $I = 1$, we arrive at the following formula for the transmission coefficient of the GMRG:

$$T = \frac{e^{-i\phi-i\xi}\left(d_{ru}^2 e^{-i\xi} + t^2 e^{-i\phi}\right) - (d_{ru}\tilde{r} - d_{tu}t)^2 e^{-i\phi} - (d_{ru}d_{tu} - r_u t)^2 e^{-i\xi}}{\left[(e^{-i\xi} - \tilde{r})(e^{-i\phi} - r_u) - d_{tu}^2\right]\left[(e^{-i\xi} + \tilde{r})(e^{-i\phi} + r_u) - d_{tu}^2\right]}. \tag{16}$$

A similar expression can be obtained for the reflection coefficient R. Let us note that no assumptions (aside from the neglected near-field effects) were made when deriving Eq. (16) (cf. Sec. III A). It is also worth mentioning that the denominator in Eq. (16) is the product of two terms corresponding to the z-symmetric and z-antisymmetric modes of the structure. Note that if the coupling coefficient d_{tu} vanishes, each of these terms itself becomes a product of two terms corresponding to the uncoupled leaky waveguide mode and Fabry-Pérot mode.

B. Bound states in the continuum

Despite the complicated form of Eq. (16), an analysis similar to the one presented in Sec. III B can be carried out. First, we equate to zero both the numerator and denominator of the fraction in Eq. (16). Then we solve the obtained system of two equations for $e^{i\phi}$ and $e^{i\xi}$, which gives us two solutions. The first solution has the form

$$e^{i\phi} = \pm\frac{t}{d_{tu}d_{ru} - r_u t}, \quad e^{i\xi} = \pm\frac{d_{ru}}{d_{tu}t - \tilde{r}d_{ru}}. \tag{17}$$

The second solution is

$$e^{i\phi} = \pm\frac{1}{\sqrt{r_u(r_u - d_{tu}^2/\tilde{r})}}, \quad e^{i\xi} = \mp\frac{1}{\sqrt{\tilde{r}(\tilde{r} - d_{tu}^2/r_u)}}. \tag{18}$$

One can show that once the matrix S is unitary, the fractions on the right-hand sides of Eqs. (17) lie on the unit circle [27]. To prove this, one should note that the inverse of the unitary matrix S calculated in terms of the adjugate matrix is equal to the conjugate transpose of the matrix S. Therefore, both ϕ and ξ in Eqs. (17) are real, which gives us a BIC. Let us note that the second solution, which is given by Eqs. (18), does not, as a rule, describe a BIC, since the moduli of the right-hand sides of Eqs. (18) are not equal to one for an arbitrary unitary scattering matrix S. However, the BICs could accidentally result from Eqs. (18) when tuning the geometrical parameters of the grating.

Let us focus on the BICs described by Eqs. (17). By applying the very same reasoning as in Sec. III B, we obtain

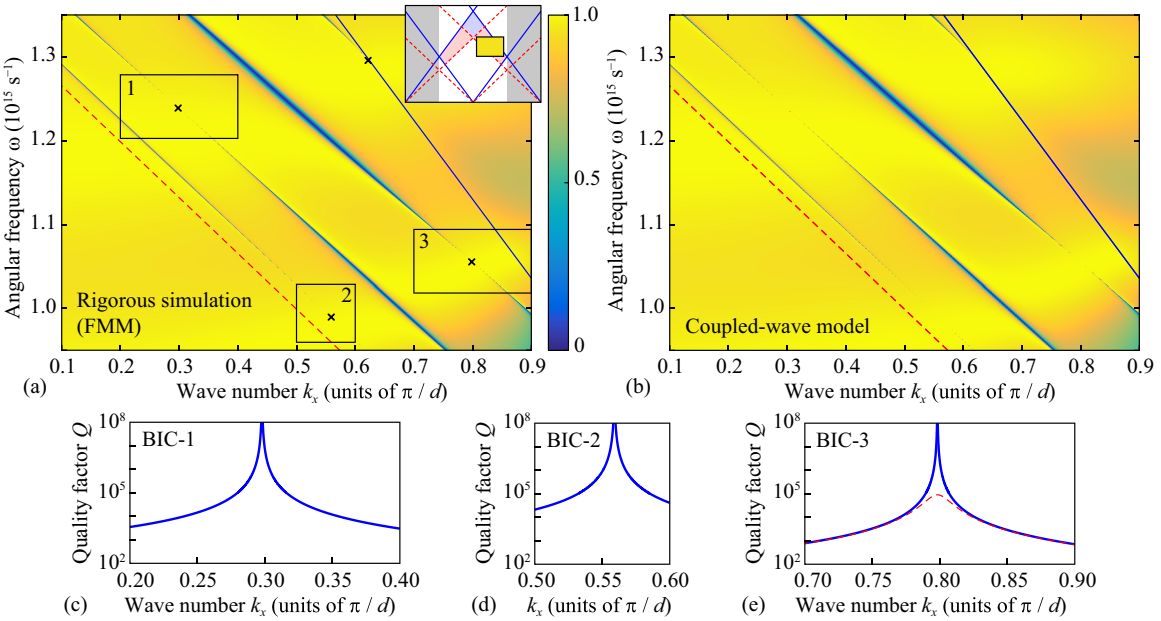

FIG. 5. (a) Rigorously calculated transmission spectrum of the considered GMRG possessing horizontal symmetry. (b) Model spectrum calculated using Eq. (16). (c)–(e) Quality factors of the modes corresponding to the fragments bounded by black rectangles. The red dashed line in (e) shows the quality factor of the modes of the GMRG having a small absorption.

the expressions for the phases

$$\phi = \pi m + \arg \frac{t}{d_{tu} d_{ru} - r_u t}, \qquad \xi = \pi l + \arg \frac{d_{ru}}{d_{tu} t - \tilde{r} d_{ru}}, \tag{19}$$

where m and l are non-negative integers having the same parity [27].

Then we solve Eqs. (3) and (13) to obtain the wave numbers and frequencies providing the BICs in the considered structure:

$$k_x = \frac{\pi}{d} + \frac{d}{4\pi h^2}(\phi^2 - \xi^2), \quad \omega = \frac{c}{n}\sqrt{k_x^2 + \frac{\xi^2}{h^2}}. \tag{20}$$

These equations describe BICs in region B_1. Similar equations can be obtained for region B_2.

C. Numerical simulations and discussion

Figure 5(a) shows the ω-k_x transmission spectrum of a GMRG with a horizontal symmetry plane. The spectrum was calculated using the FMM. The parameters of the binary gratings and WG layer are the same as in Sec. III D. The spectrum contains four pronounced resonant curves, each one having a BIC. Figure 5(b) shows the model spectrum calculated using Eq. (16). The model spectrum agrees perfectly with the rigorously calculated one, which confirms the accuracy of the coupled-wave model of Sec. IV A.

Figures 5(c)–5(e) show the quality factor of the modes. The ranges of the Q-factor plots coincide with the black rectangles in Fig. 5(a). The divergence of the Q factor in these plots confirms that the considered structure supports BICs.

In order to verify the BIC model presented in Sec. IV B, we calculated the BIC positions using Eqs. (19) and (20). The predicted (ω, k_x) points are marked in Fig. 5(a) with black crosses. The predicted BIC positions are in excellent agreement with the results of the rigorous simulations.

It is interesting to discuss how a small absorption in the material of the GMRG affects the BICs. Once we add a small imaginary part ($k = 10^{-5}$) to the refractive index of the structure, all the BICs collapse to high-Q Fano resonances (quasi-BICs). We demonstrate this by calculating the quality factor of the (quasi-)BIC-3, which is shown in Fig. 5(e) with a red dashed line. This plot demonstrates a high but finite value of the quality factor Q. Concerning the presented coupled-wave model, in the absorbing structure, the magnitudes of the exponents in Eqs. (17) are no longer unity. However, Eqs. (19) and (20) can still be used to estimate the quasi-BIC positions. For the considered example, these positions are visually indistinguishable from the BIC positions marked by the black crosses in Fig. 5(a) corresponding to the lossless structure.

Let us note that the models presented in the current and in the previous sections are quite similar. Indeed, we use either Eq. (9) or Eqs. (17) to describe the BIC positions. To prove the BIC existence, we show that the right-hand sides of these equations have unit magnitude by using the consequences of the unitarity of the scattering matrix S. At the same time, the BIC formation mechanisms for the two considered cases are quite different. Indeed, in the case of region A, the BICs (and quasi-BICs) emerge at the avoided crossings of the dispersion curves (see Fig. 3). This anticrossing indicates strong coupling between the waveguide modes having comparable Q factors. However, in region B considered in this section, the Fabry-Pérot modes have significantly lower quality factors. Consequently, the coupling between a waveguide mode and a Fabry-Pérot mode is weaker in this case, and no avoided crossings are present in Fig. 5. Nevertheless, both the model and the simulation results demonstrate that even this weak coupling provides the formation of the BICs.

V. CONCLUSION

In this paper we investigated bound states in the continuum supported by lossless guided-mode resonant gratings comprising a slab waveguide and a binary grating attached to one or both of its interfaces. Two mechanisms behind the BIC formation were studied: the coupling of two counterpropagating waveguide modes and the coupling of a waveguide mode with a Fabry-Pérot mode. In both cases, the BICs (or quasi-BICs) arise due to multiwave interference of light inside the slab. We formulated accurate coupled-wave models, which rigorously prove the BIC existence and predict their locations in the ω-k_x plane. The BIC existence proof exploits the energy conservation law, resulting in the unitarity of the scattering matrix of the binary grating. The rigorous simulation results confirm the high accuracy of the presented models.

The formulated models suggest that the existence of the BICs is closely connected with the symmetry properties of the gratings and hence with the form of their scattering matrices. In our opinion, models similar to the ones presented here can be developed for GMRGs possessing different symmetries. For example, the model of Sec. IV can be applied with minimal modifications when the lower grating is laterally shifted with respect to the upper one, thus breaking the horizontal symmetry. In this case, the corresponding elements of the scattering matrices S in Eqs. (14) and (15) will acquire different phases, with the difference depending on the lateral shift introduced between the gratings.

Finally, let us outline a few other directions for the further research. We believe that similar models can be formulated for different parameter spaces: Instead of the (ω, k_x) pair, one can consider (θ, h) or even (k_y, h), with the latter corresponding to the case of purely conical diffraction (nonzero k_y at $k_x = 0$).

We also believe that the main results of Sec. IV can be used to describe BICs in high-contrast gratings (HCGs). These structures were shown to support high-Q resonances in the so-called two-mode regime, when the field inside the grating can be approximately represented as a superposition of two pairs of waves, which are the modes of a 1D photonic crystal [39,40]. Similarly to the mechanism described in the present work, these two modes are coupled at the upper and lower interfaces of the HCG. Therefore, we expect that Eqs. (14)–(19) can be used to describe BICs in HCGs. In this case, an analog of Eq. (20) will be based on the dispersion relation of a 1D photonic crystal.

ACKNOWLEDGMENTS

This work was funded by Russian Foundation for Basic Research (Projects No. 18-37-20038 and No. 16-29-11683, coupled-wave models) and by Ministry of Science and Higher Education of the Russian Federation (state contract with the FSRC Crystallography and Photonics RAS under agreement 007-GZ/Ch3363/26, numerical simulations).

[1] J. von Neumann and E. Wigner, Über merkwürdige diskrete eigenwerte, Phys. Z. **30**, 465 (1929).

[2] C. W. Hsu, B. Zhen, A. D. Stone, J. D. Joannopoulos, and M. Soljačić, Bound states in the continuum, Nat. Rev. Mat. **1**, 16048 (2016).

[3] H. Friedrich and D. Wintgen, Interfering resonances and bound states in the continuum, Phys. Rev. A **32**, 3231 (1985).

[4] D. C. Marinica, A. G. Borisov, and S. V. Shabanov, Bound States in the Continuum in Photonics, Phys. Rev. Lett. **100**, 183902 (2008).

[5] E. N. Bulgakov, D. N. Maksimov, P. N. Semina, and S. A. Skorobogatov, Propagating bound states in the continuum in dielectric gratings, J. Opt. Soc. Am. A **35**, 1218 (2018).

[6] E. N. Bulgakov and A. F. Sadreev, Bloch bound states in the radiation continuum in a periodic array of dielectric rods, Phys. Rev. A **90**, 053801 (2014).

[7] Z. F. Sadrieva and A. A. Bogdanov, Bound state in the continuum in the one-dimensional photonic crystal slab, J. Phys.: Conf. Ser. **741**, 012122 (2016).

[8] J. W. Yoon, S. H. Song, and R. Magnusson, Critical field enhancement of asymptotic optical bound states in the continuum, Sci. Rep. **5**, 18301 (2015).

[9] Z. F. Sadrieva, I. S. Sinev, K. L. Koshelev, A. Samusev, I. V. Iorsh, O. Takayama, R. Malureanu, A. A. Bogdanov, and A. V. Lavrinenko, Transition from optical bound states in the continuum to leaky resonances: Role of substrate and roughness, ACS Photon. **4**, 723 (2017).

[10] C. W. Hsu, B. Zhen, J. Lee, S. L. Chua, S. G. Johnson, J. D. Joannopoulos, and M. Soljačić, Observation of trapped light within the radiation continuum, Nature (London) **499**, 188 (2013).

[11] S. I. Azzam, V. M. Shalaev, A. Boltasseva, and A. V. Kildishev, Formation of Bound States in the Continuum in Hybrid Plasmonic-Photonic Systems, Phys. Rev. Lett. **121**, 253901 (2018).

[12] S. P. Shipman and S. Venakides, Resonant transmission near nonrobust periodic slab modes, Phys. Rev. E **71**, 026611 (2005).

[13] D. A. Bykov and L. L. Doskolovich, ω-k_x Fano line shape in photonic crystal slabs, Phys. Rev. A **92**, 013845 (2015).

[14] C. Blanchard, J.-P. Hugonin, and C. Sauvan, Fano resonances in photonic crystal slabs near optical bound states in the continuum, Phys. Rev. B **94**, 155303 (2016).

[15] E. N. Bulgakov and D. N. Maksimov, Avoided crossings and bound states in the continuum in low-contrast dielectric gratings, Phys. Rev. A **98**, 053840 (2018).

[16] B. Zhen, C. W. Hsu, L. Lu, A. D. Stone, and M. Soljačić, Topological Nature of Optical Bound States in the Continuum, Phys. Rev. Lett. **113**, 257401 (2014).

[17] E. N. Bulgakov and D. N. Maksimov, Bound states in the continuum and polarization singularities in periodic arrays of dielectric rods, Phys. Rev. A **96**, 063833 (2017).

[18] E. N. Bulgakov and D. N. Maksimov, Topological Bound States in the Continuum in Arrays of Dielectric Spheres, Phys. Rev. Lett. **118**, 267401 (2017).

[19] L. Yuan and Y. Y. Lu, Strong resonances on periodic arrays of cylinders and optical bistability with weak incident waves, Phys. Rev. A **95**, 023834 (2017).

[20] C. W. Hsu, B. Zhen, S.-L. Chua, S. G. Johnson, J. D. Joannopoulos, and M. Soljačić, Bloch surface eigenstates within the radiation continuum, Light Sci. Appl. **2**, e84 (2013).

[21] E. N. Bulgakov and A. F. Sadreev, Bound states in the continuum in photonic waveguides inspired by defects, Phys. Rev. B **78**, 075105 (2008).

[22] I. V. Timofeev, D. N. Maksimov, and A. F. Sadreev, Optical defect mode with tunable Q factor in a one-dimensional anisotropic photonic crystal, Phys. Rev. B **97**, 024306 (2018).

[23] Y. Plotnik, O. Peleg, F. Dreisow, M. Heinrich, S. Nolte, A. Szameit, and M. Segev, Experimental Observation of Optical Bound States in the Continuum, Phys. Rev. Lett. **107**, 183901 (2011).

[24] M. I. Molina, A. E. Miroshnichenko, and Y. S. Kivshar, Surface Bound States in the Continuum, Phys. Rev. Lett. **108**, 070401 (2012).

[25] S. Weimann, Y. Xu, R. Keil, A. E. Miroshnichenko, A. Tünnermann, S. Nolte, A. A. Sukhorukov, A. Szameit, and Y. S. Kivshar, Compact Surface Fano States Embedded in the Continuum of Waveguide Arrays, Phys. Rev. Lett. **111**, 240403 (2013).

[26] C.-L. Zou, J.-M. Cui, F.-W. Sun, X. Xiong, X.-B. Zou, Z.-F. Han, and G.-C. Guo, Guiding light through optical bound states in the continuum for ultrahigh-Q microresonators, Laser Photon. Rev. **9**, 114 (2015).

[27] E. A. Bezus, D. A. Bykov, and L. L. Doskolovich, Bound states in the continuum and high-Q resonances supported by a dielectric ridge on a slab waveguide, Photon. Res. **6**, 1084 (2018).

[28] D. A. Bykov, E. A. Bezus, and L. L. Doskolovich, Topologically protected bound states in the continuum and strong phase resonances in integrated Gires-Tournois interferometer, arXiv:1904.06939.

[29] A. Kodigala, T. Lepetit, Q. Gu, B. Bahari, Y. Fainman, and B. Kanté, Lasing action from photonic bound states in continuum, Nature (London) **541**, 196 (2017).

[30] S. T. Ha, Y. H. Fu, N. K. Emani, Z. Pan, R. M. Bakker, R. Paniagua-Domínguez, and A. I. Kuznetsov, Directional lasing in resonant semiconductor nanoantenna arrays, Nat. Nanotechnol. **13**, 1042 (2018).

[31] M. Rybin and Y. Kivshar, Supercavity lasing, Nature (London) **541**, 164 (2017).

[32] Y. Liu, W. Zhou, and Y. Sun, Optical refractive index sensing based on high-Q bound states in the continuum in free-space coupled photonic crystal slabs, Sensors **17**, 1861 (2017).

[33] S. Romano, G. Zito, S. Torino, G. Calafiore, E. Penzo, G. Coppola, S. Cabrini, I. Rendina, and V. Mocella, Label-free sensing of ultralow-weight molecules with all-dielectric metasurfaces supporting bound states in the continuum, Photon. Res. **6**, 726 (2018).

[34] J. M. Foley, S. M. Young, and J. D. Phillips, Symmetry-protected mode coupling near normal incidence for narrow-band transmission filtering in a dielectric grating, Phys. Rev. B **89**, 165111 (2014).

[35] N. A. Gippius, S. G. Tikhodeev, and T. Ishihara, Optical properties of photonic crystal slabs with an asymmetrical unit cell, Phys. Rev. B **72**, 045138 (2005).

[36] D. A. Bykov and L. L. Doskolovich, Numerical methods for calculating poles of the scattering matrix with applications in grating theory, J. Lightw. Technol. **31**, 793 (2013).

[37] M. G. Moharam, E. B. Grann, D. A. Pommet, and T. K. Gaylord, Formulation for stable and efficient implementation of the rigorous coupled-wave analysis of binary gratings, J. Opt. Soc. Am. A **12**, 1068 (1995).

[38] L. Li, Formulation and comparison of two recursive matrix algorithms for modeling layered diffraction gratings, J. Opt. Soc. Am. A **13**, 1024 (1996).

[39] V. Karagodsky, C. Chase, and C. J. Chang-Hasnain, Matrix Fabry-Perot resonance mechanism in high-contrast gratings, Opt. Lett. **36**, 1704 (2011).

[40] V. Karagodsky and C. J. Chang-Hasnain, Physics of near-wavelength high contrast gratings, Opt. Express **20**, 10888 (2012).